

Comparative theoretical study of the size dependent electronic and optical properties in CdS and CdSe spherical nanocrystals

Amjad Nazzal and Huaxiang Fu*

Department of Physics, University of Arkansas, Fayetteville, Arkansas 72701, USA

(Dated: July 31, 2008)

Abstract

We present a comparative study on the quantum size effects in CdS and CdSe spherical dots, using first-principles derived semi-empirical pseudopotential method. Various properties including single-particle energy levels, characterization of individual electron wave functions, interband and intraband transitions, electron-hole Coulomb and exchange interactions, and excitonic band gap are investigated. The similarity and difference between CdSe and CdS dots are discussed. Our specific findings are rather lengthy, and are summarized in Section IV.

Keywords: CdS nanocrystals, CdSe nanocrystals, electronic structure, optical properties.

*Corresponding author, Email: hfu@uark.edu, Telephone: 479-575-8608, Fax: 479-575-4580.

I. INTRODUCTION

Quantum dots (QDs) made of CdSe, and to a less extent, CdS, are considered as model systems for scientists to test their theoretical approaches [1–14]. They favor these systems because of the existence of wealthy collection of experimental data [15, 16] available for both CdSe and CdS nanocrystals (NCs). Rapid developments in spectroscopic techniques have enabled characterization of individual energy states of the electronic spectrum [17, 18]. This experimental advance was in part propelled by the remarkable level of control over the synthesis developed in the last decade to grow high-quality colloidal NCs of CdSe and CdS [19–21].

As *bulk* materials, CdSe and CdS exhibit differences as well as similarities. Under ambient conditions, both CdSe and CdS adopt the hexagonal Wurtzite structure with inplane lattice constant $a_0=4.30\text{\AA}$ (4.14\AA) and out-of-plane constant $c_0=7.01\text{\AA}$ (6.72\AA) for CdSe (CdS). The same crystal structure leads to similar electronic band structure and hence electronic properties in these direct-gap materials. The band gap in bulk CdS is ~ 2.5 eV, about 0.65 eV larger than in CdSe. However, a noticeable difference between these two semiconductors is the bulk exciton Bohr radius (R_{ex}) which is around 55\AA in CdSe, about twice the value of CdS (25\AA) [22]. As a result, the binding energy of bulk exciton in CdSe (12 meV) is considerably smaller than that in CdS (28 meV). The large difference in their R_{ex} radii is due to: (i) the high frequency limit of the dielectric function $\epsilon^{bulk}(\infty)$ in CdSe which is 6.25, compared to 5.32 in CdS, (ii) the heavy-hole mass is 0.45 in CdSe and 0.7 in CdS. Another key difference between two semiconductors is the spin-orbit coupling, which is very large in CdSe (0.42 eV) but markedly little in case of CdS (0.068 eV).

Considerable differences, exhibited by bulk CdSe and CdS of the same crystal structure, naturally lead scientists to wonder how different and/or similar the properties of these two substances will be when they are made into low-dimensional structures. More specifically, one may ask which semiconductor may show a larger size-induced shift in exciton band gap, and by how much, provided that the size of nanocrystal is the same for two materials. Meanwhile, it is of interest to find out how the exciton Coulomb binding may differ in CdSe and in CdS nanocrystals. In addition to electronic properties, optical transition is another quantity of great technological relevance for semiconductor quantum-dot laser and other device applications. Given the same size, which semiconductor dot (CdSe or CdS) has

larger intensity in terms of band-edge transition? Further, how does the relative intensity between CdSe and CdS dots depends on, and thus can be influenced by, the size.

Nowadays it has been made possible in real experiments to access and differentiate individual energy levels [23–25], thereby allowing one to trace and characterize the confinement effect on each energy level in QDs. One interesting problem concerns the intriguing nature of the valence band maximum (VBM) of CdS dots. A combined study of experimental measurement and theoretical calculation [17] revealed that the angular momentum of the *envelope* function component of the top valence state has a p symmetry ($1P_{1/2}$) for CdS dots smaller than $D = 14$ nm in diameter. The VBM in QDs with diameter larger than this size was found to have a different envelope function, with instead an s -symmetry ($1S_{3/2}$). The spatial difference between the VBM and the conduction band maximum (CBM) in symmetry of envelope functions leads to an exciton ground state that is optically passive for CdS QDs with diameter $D < 14$ nm. This is in sharp contrast to the case of CdSe QDs, where the VBM is found to be bright for all sizes [23]. The theory of p -symmetry VBM was used to explain the significant difference exhibited in the resonant Stokes shift observed experimentally in CdS QDs [17]. However, a more recent calculation by Demchenko and Wang employing the local density functional derived charge patching method led to a different conclusion [26]; they found that the Stokes shift could be interpreted as a result of the electron-hole exchange interaction which induces a spin-forbidden dark exciton rather than the spatial symmetry forbidden dark exciton. This latter study reinstates that the hole ground state is a bright state ($1S_{3/2}$), not a dark P -state as predicted previously by the $\mathbf{k}\cdot\mathbf{p}$ method. The exciton is thus not spatially forbidden in CdS quantum dot. In this context, the level ordering and the nature of the band edge states, particularly the VBM in CdS QDs, is still unsettled.

The experimental advance in optical spectroscopy of semiconductor dots has also generated interest in another problem, centering on the contributions of individual shifts of the CBM and VBM to the size induced band-gap opening. For example, in Si nanocrystals, experimental observations demonstrated that the size induced shifts in the band-edge states are more pronounced for the VBM rather than for the CBM [27], which was confirmed by theory [28] and is consistent with the X-like nature of the VBM in Si. For CdS quantum dots, experimental measurements determined that the opening of the band gap is equally contributed by the VBM as by the CBM. [29] Meanwhile, the authors also expressed their concerns about the effect of the surface treatment on the behavior of these shifts [29]. A

recent TB calculation [14] performed on CdS and CdSe QDs has shown, however, that the CBM contribution is many folds larger than that of the VBM, especially for CdS QDs. On the one hand, the fact that individual band contribution to the band gap opening is vastly dominated by the upward shift of the CBM rather than the downward shift of the VBM in dots made of either CdSe or CdS can be simply explained by use of electron and hole masses. In both materials electron mass m_e^* is far less than m_h^* of hole; more specifically, $m_e^*=0.13$ and $m_h^*=0.45$ for CdSe, and $m_e^*=0.17$ and $m_h^*=0.70$ for CdS [22]. On the other hand, the simple estimation based on carrier mass does not address the problem quantitatively, particularly if one needs to determine (1) What is the ratio between the upshift of CBM and the downshift of the VBM, in contributing to the band-gap widening? (2) How this ratio varies with the size? To answer quantitatively these questions one would need reliable theoretical tools.

Moreover, there is a third issue of interest, concerning the *intraband* transitions in CdSe and CdS dots. CdSe and CdS are commonly known as moderate and/or wide-gap materials, and thus one would inevitably focus on optical applications in the visible or ultraviolet energy regions. However, modern engineering of nanocrystal structures could open doors for new applications in the near-or-mid infrared regions. For example, developing methods that utilize the intraband optical transitions (in a similar sense to the technology used in cascade lasers) would be one potential possibility, due to the available dense spectrum of energy states inside the valence and/or conduction bands. Control over the tunability of these energy states will be a desirable advantage for these infrared applications. While the intraband transitions in CdSe dots was amply investigated[30], it would be of interest to make a comparative study in CdS nanocrystals. One question of relevance is how the intraband transition intensity in CdS dots is enhanced or decreased as compared to CdSe dots, and which dots are more suitable for infrared devices. Since the intraband transition intensity must be size dependent, one may pose a more intriguing question, that is, whether there is any size that may be particularly useful for infrared applications by displaying maximized intraband intensity.

The shape of semiconductor nanocrystals is known to play an important role in determining their electronic and optical properties. For example, sufficiently elongated CdSe rods were shown to produce differently polarized emission as compared to spherical dots.[8] On the electronic band gap, a previous theoretical study showed that the spherical shape has the

smallest band gap when compared to other elongated shapes of CdSe NCs containing similar number of atoms.[31] However, another study on CdS NCs of different geometries using a Wannier function approach [32] showed that the band gap of the NC is almost independent of the shape.

It is our objective of this study to address the electronic structure of CdSe and CdS QDs, based on the same footing. We use local-density functional derived, with band gap empirically corrected, screened pseudopotentials (termed as semi-empirical pseudopotential method or SEPM). We consider quantum dots of spherical geometry in this comparative study, which seems more suitable and represents a good starting point. First, being most compacted object, spherical dots impose no alteration of symmetry to electron wavefunctions as compared to the symmetry group in bulk wurtzite semiconductors. Second, spherical dots allow us to concentrate on size effects by isolating the shape influence. In this study of two dissimilar (but of alike crystal structure) Cd chalcogenides, we wish to understand several key issues of interest to both experiments and theories: 1) One-body properties: characterization of single-particle energy levels and wavefunction symmetries in both types of dots, and the complex level ordering as a function of size, (2) Two-body properties: influences of size on the electron-hole (Coulomb and exchange) interactions and the excitonic band gap, (3) Optical transitions: interband and intraband optical excitations.

II. THEORETICAL METHODS

Ideally, one would prefer a direct first-principles density functional theory (DFT) [33] to describe electron properties of semiconductor nanostructures. Direct DFT calculations allow one to account for the charge redistribution that may take place both inside and at the surfaces of nanostructures. To study optical properties, one would also encounter another obstacle, which is the underestimation of the local density approximation (LDA) on band gap. One thus further desires to conduct quasi-particle calculations[34] so that a direct comparison is possible between theoretical and experimental energies of optical excitation. However, nanostructures of interest often contain several thousands (sometimes millions) of atoms. Computational studies of these structures by direct first-principles approaches are generally very time consuming, which limits the application only to dots or wires of small size.[35–37] Alternative approaches, other than the direct DFT calculations, take advan-

tage of the fact that a majority of real experiments have been performed on nanostructures that are passivated by organic capping materials or by other semiconductor shells. Nanostructures with passivation tend to provide better and controllable optical properties. The passivation removes, electrostatically and/or chemically, defect states away from the fundamental band edge. In fully passivated dots or wires, measured properties mainly originate from the spatial interior of the structures and subject only little variation to surface conditions. This is often preferred since the bulklike properties are intrinsic and can be effectively controlled. Surface effects in semiconductor nanostructures, while interesting, vary from sample to sample, however. For fully-passivated semiconductor nanostructures, alternative approaches to determine their electronic structure include charge patching method,[38] tight-binding linear combination of atomic orbits,[39–41] pseudopotentials,[42–44], or multiband k·p theory.[45, 46]. Here we use the semi-empirical pseudopotential method (SEPM). The accuracy of SEPM has been amply demonstrated by numerous previous applications of this method to study the electronic structure and optical properties of different II-VI and III-V quantum dots[7, 47–51].

In SEPM, the single particle wave function and energy are obtained by solving the Schrödinger equation through direct diagonalization of the following folded Hamiltonian [42]

$$\left[-\frac{\hbar^2}{2m_0} \nabla^2 + V_{ps}(\mathbf{r}) + V_{nl} + V_{so}(\mathbf{r}) - \epsilon_{ref}\right] \psi_i(\mathbf{r}) = (\epsilon_i - \epsilon_{ref}) \psi_i(\mathbf{r}), \quad (1)$$

where the microscopic local pseudopotential $V_{ps}(\mathbf{r})$ is the superposition of screened atomic potentials (v_{SEPM}) of all atoms contained in the structure, V_{nl} the short-range non-local part of the pseudopotential, V_{so} the potential describing spin-orbit interaction. Screened atomic potentials (v_{SEPM}) are derived from first-principles local density functional calculations on bulk CdSe and CdS, using a scheme similar to the method that was used to generate the SEPM potential for InP in Ref.47. Obviously, the LDA-derived screened atomic potential will inherit the drawback of LDA by underestimating band gap. To correct it, the screened potential is then parameterized and the parameters are adjusted to reproduce the experimental band gap, effective mass, and work function. For CdSe (but not for CdS), there is an early version of SEPM potential in the literature[7]. In order to be able to handle CdSe and CdS on an equal footing, we nevertheless decide to regenerate independently the SEPM potential for CdSe as well as for CdS. Our SEPM potentials for CdSe and CdS reproduce well the experimental band gaps, electron and hole effective masses, and band

dispersions. In Eq.(1), the single-particle pseudopotential wavefunctions are expanded in a plane-wave basis set; more specifically, for the Γ -point of quantum-dot states, $\psi_i(\mathbf{r}) = \sum_{\mathbf{G}} c_i(\mathbf{G}) \exp(i \mathbf{G} \cdot \mathbf{r})$, where the sum runs over the reciprocal lattice vectors of the supercell. Cubic supercells that contain the spherical nanocrystals plus sufficient vacuum region along the x , y and z directions are used. The expansion coefficients are obtained by minimizing the functional $A[\psi] = \langle \psi | (\hat{H} - \epsilon_{ref})^2 | \psi \rangle$ using a preconditioned conjugate-gradient algorithm [52]. After determining the one-body electron levels ϵ_i and wavefunctions ψ_i in Eq.(1), the Coulomb and exchange interactions between electron and hole are computed using these realistic wavefunctions and with screening effect taken into account. The exciton spectrum is further obtained within the framework of configuration interaction, by use of Slater determinant constructed from the pseudopotential single-particle wavefunctions. Specific scheme of this approximation is similar to Ref.50.

Both CdSe and CdS have the hexagonal Wurtzite structure whose cell shape and internal parameters are close to the ideal values $c/a=1.633$ and internal parameter $u=0.376$. We use LDA calculated bulk inplane lattice constants of $a_0(\text{CdSe})=4.23\text{\AA}$ and $a_0(\text{CdS})=4.08\text{\AA}$. For nanocrystals, six different sizes of the spherical shape are considered, with the radius (r) ranging from 2.0 to $4.5a_0$ in units of lattice constant. By using the number of atoms contained in the dot, the effective diameter D is calculated to be from 16.94 to 38.12\AA for CdSe dots, and from 16.32 to 36.72\AA for CdS dots.

Surface atoms with dangling bonds are passivated by pseudo-hydrogen like potentials of the gaussian form:

$$V(r) = V_0 \exp\left[-\frac{|\vec{r} - \vec{R}|^2}{d^2}\right], \quad (2)$$

where V_0 , d and R specify the height, width and center of the potential. These parameters were varied and determined using CdSe and CdS thin films up to 15 monolayers along the 001 and 110 directions, so that all surface states of these films are pushed out of the band gap. The optimized parameters were then tested on a real nanocrystal for confirmation check, and the effect of this passivation on bulk states was investigated in terms of energy, spatial distribution, bulk Bloch-states decomposition, etc., to make sure that the passivation works well. When constructing nanocrystal surfaces, we ignore surface reconstruction that may occur for unpassivated dots like the one considered in Ref.[53]. We believe that complete passivation minimizes possible surface reconstructions by eliminating the interaction

between dangling bonds. Table IV shows the optimized passivation parameters used in our calculations for the surface atoms with one and two dangling bonds; surface atoms with three dangling bonds are less stable and are eliminated in our procedure of constructing nanocrystal surfaces.

III. RESULTS AND DISCUSSION

Our calculated band structures, obtained from the SEPM, are shown in Fig.1 for bulk CdSe and CdS. The theoretical direct band gap at Γ -point turns out to be 1.77 (2.54) eV for CdSe (CdS), in good agreement with the experimentally reported value of 1.84 (2.58) eV [22]. The calculated spin-orbit splitting in CdSe is 0.39 eV, as compared to 0.08 eV in CdS. The single-particle orbital energies at special \mathbf{k} points (Γ , M, and A), electron and hole effective masses, and the overall band dispersions in Fig.1 all agree well with experiments or quasi-particle GW calculations.

In Fig.2, we present the calculated single-particle eigenvalues of conduction and valence electron states of the CdSe and CdS QDs at the studied sizes. Ten conduction states and ten valence states near the band edge are given for each size. In regard to the size evolution of the single-particle energy levels, our main observations are:

(1) The conduction states have similar structure in both types of QDs. The CBM is separated from the next group of three states (i.e., CBM+1, CBM+2 and CBM+3) by an intraband gap, to be denoted as $\Delta E_{\text{intra,CB}}^{(1)}$. CBM+1 and CBM+2 are separated by few meVs, and can not be distinguished in Fig.2, while CBM+2 separates from CBM+3 by tens of meVs. The $\Delta E_{\text{intra,CB}}^{(1)}$ intraband gap decreases by half with the increasing size in an almost linear fashion, starting from ~ 0.7 (0.6) eV in the smallest CdSe (CdS) QD down to ~ 0.35 (0.3) eV for the largest CdSe (CdS) QD. Interestingly, in addition to the $\Delta E_{\text{intra,CB}}^{(1)}$ intraband gap, we notice that a second quasi-gap, termed as $\Delta E_{\text{intra,CB}}^{(2)}$, significantly develops at size $r=3.0a_0$ for both CdSe and CdS dots, which separates the four lowest conduction states from the higher ones. $\Delta E_{\text{intra,CB}}^{(2)}$ fluctuates around an average value of 300 meV for the size range $r=3.0\sim 4.5a_0$. Comparing the two quasi-gaps [$\Delta E_{\text{intra,CB}}^{(1)}$ versus $\Delta E_{\text{intra,CB}}^{(2)}$], we find that as size increases, the first intraband gap shrinks at a faster rate that brings it close to the value of the second one, and we expect that at larger sizes beyond the range of our study, the second gap will become the dominating intraband gap in the CBs. Indeed,

for the CdS QD of size $r=4.0 a_0$, the $\Delta E_{\text{intra,CB}}^{(2)}$ gap exceeds the $\Delta E_{\text{intra,CB}}^{(1)}$ gap by around 25.0 meV. The observed similarities in the conduction states of two types of dots could be attributed to the alike conduction-band dispersions of their bulk substances, which results in similar dynamics with size confinement.

(2) However, and unlike the electron spectrum, the energy distribution of the hole levels is fairly different in CdSe dots and in CdS dots. Let us examine CdSe dots first, and then move to CdS dots. For CdSe dots, (i) the most noticeable feature of their valence-state spectrum is the formation of an intraband gap, denoted as $\Delta E_{\text{intra,VB}}$, separating the four highest VB states (which form a group) from the other six lower states. As shown in Fig.3, for the CdSe QDs (filled squares), this quasi gap is nearly unchanged for the smallest three sizes (about 175 meV) and then linearly drops to around 90 meV for the largest QD. Our calculations thus reveal that the size of intraband gap of valence states is far smaller than that of the conduction states in CdSe dots, namely being 90 meV versus 350 meV in the $r=4.5a_0$ dot. Note that the energy scale of the vertical axis in Fig.2 is not the same for conduction states as for valence states. Meanwhile, it is rather unusual that the $\Delta E_{\text{intra,VB}}$ of CdSe dots is size insensitive for three smallest dots, since one generally expects the energy difference should be influenced by size. (ii) We further show, in the inset of Fig.3, the energy separation between the VBM and the next highest valence state, VBM-1. The separation fluctuates strongly as a function of the QD size, without displaying a monotonic behavior as expected. For the largest four sizes, its value is around 20 meV and then sharply increases by more than 100% for the smallest two QDs. This abrupt change of behavior is an evidence of strong interstate mixing between valence states, and as an outcome, the change in the nature of these states due to level crossing that leads to different structure of spectrum as size evolves. (iii) To better understand the level crossing, one has to study the individual wavefunctions of the hole states, whose spatial distributions are given in Fig.4. The wave functions of the same character are shown in the same row in Fig.4. The first row of Fig.4, from left to right, traces how the VBM of the largest $r=4.5a_0$ dot evolves as size decreases. The state of this character remains to be the VBM in dots of other sizes until $r=2.5a_0$. However, when size continues to decrease to $r=2.0a_0$, this state is no longer the VBM. Instead, it becomes VBM-1. Another state of different character (see the third plot of the second row in Fig.4) rises to be the VBM at $r=2.0a_0$. The second row of Fig.4 tells us what state in the larger dot becomes the VBM of the smallest size, in other words, it traces the

origin of the VBM of the smallest size. We see, from right to left in the second row of Fig.4, that the VBM of the $r=2.0a_0$ dot emerges from the VBM-1 of the $r=2.5a_0$ QD which in turn originates from the VBM-3 of the $r=4.5a_0$. The VBM in the smallest size of $r=2.0a_0$ is thus a completely different state from all the other sizes where the VBM is found to be the same in the size range from $r=2.5$ to $4.5a_0$. Further changes in the ordering of the hole states are shown in the third row of Fig.4, displaying the evolution of the VBM-1 state of the largest $r=4.5a_0$ dot as the size decreases. It evolves into the VBM-3 in $r=3.5a_0$ and then into the VBM-2 in $r=3.0a_0$. These multiple level crossings are complex, and are responsible for the non-monotonous variation of the energy separation between the VBM and VBM-1 in the inset of Fig.3, since they correspond to different states in different sizes. The level crossing is due to, in light of the fact that the geometric shape of the system is preserved, different spatial distributions of individual hole states. When the boundary of dot changes (as in different sizes of dots), these states are affected differently. For CdSe dots, the top four valence states behave similarly, explaining their grouping and hence the appearance of the quasi-gap in the hole spectrum.

For the hole spectrum in CdS, the situation is different. In the lower panel of Fig.2, it is evident that for the smallest three QDs, the highest 6 VB states form a group that is separated from the lower 4 states by a pseudo-gap. This intraband gap in CdS evolves in a different manner than the one discussed for CdSe. As shown on Fig.3, this intraband gap, referred to as IG1, is around 160 meV for the smallest two QDs. As size increases, this intraband gap almost disappears and is hardly seen in Fig.2. By following the evolution of this intraband gap through analysis of wave functions, we find that it drops significantly by an order of magnitude to ~ 10 meV in the largest QD. In the meantime, another intraband gap (that is different from the IG1, and that is to be referred to as IG2) becomes evident in Fig.2 for $r=4.0a_0$ and $r=4.5a_0$ dots. The IG2 intraband gap separates the highest 4 VB states from the rest states below them. The IG2 gap is around 50 meV and does not vary appreciably with the nanocrystal size for the largest four sizes (Fig.3). From Fig.3, we thus see that in the size range from $D=25\text{\AA}$ to $D=35\text{\AA}$, the intraband gap of valence states in CdS differs considerably from that in CdSe. Analysis of spatial distribution of the wavefunctions reveals that the VBM in CdS dots does not alter its character for all the sizes considered in this study. However, the VBM-1 was found to undertake several level crossings. More specifically, the VBM-1 in the largest two QD sizes is changed into the VBM-2 in $r=3.5a_0$

and eventually becomes the VBM-3 in the smallest QD. For CdS dots of all sizes, we find that the VBM has s -like envelop symmetry, and is transition allowed. The VBM-1 of $r=4.5a_0$ has a p -like envelop symmetry, with the maximum wavefunction amplitude not at the center of the dot. When size shrinks, the p -like valence state is modified more than the s -like state, since the wavefunction peak location of the former is closer to the dot boundary than the latter, and is pushed harder by the confinement. One possible reason for the significant difference in the valence states between CdS and CdSe dots is the large spin-orbit interaction in CdSe, which *reduces* the interstate coupling by separating the spin split band from the higher valence bands.

(3) The shifts of the CBM and the VBM in dots with respect to the band-edge energies in bulk, $\delta = |\varepsilon_i^{\text{Dot}} - \varepsilon_i^{\text{Bulk}}|$, are generally described analytically by the form

$$\delta = \frac{\beta}{D^\alpha} . \quad (3)$$

We have fitted the relative shifts of the VBM and the CBM (in eV) as a function of the diameter D (in Å) using the above expression, by varying α and β using a least square fitting procedure. The fitting results turn out to be a good description of the directly calculated data (deviation in the fitting parameters is within few percent). The obtained parameters are given in Table IV. In CdSe, the α values are between 1.0 and 2.0 for both CBM and VBM, revealing the expected competition between potential energy ($1/D$) and kinetic energy ($1/D^2$). Notably, the scaling α exponent of the VBM states in CdS dots, $\alpha = 2.2$, exceeds the value $\alpha=2$ expected from the model of “particle in a box” that has the strongest confinement. This is rather puzzling. As we discussed above, the VBM state in CdS dots does not change its nature and spatial symmetry of the envelope function in the size range considered in our study, and thus we can not explain the behavior of anomalous α as a phenomenon arising from contribution of different states. In fact, the obtained $\alpha > 2$ exponent is an indication of strong interstate coupling. In the large dots, strong interstate repulsion pushes the VBM upper than it should be in the single-band case (i.e., the case of no coupling). In small dots, the interstate coupling is small due to the large energy separation. As an overall effect that combines quantum confinement and interstate coupling, the VBM decreases more rapidly with the size than the prediction by the model of a particle of single-band in an infinite potential barrier, leading to $\alpha > 2$. In addition to the α exponent, it is also useful to point out a misunderstanding about the β values. Naively, one may think that the β value should

be inversely proportional to the effective mass. But our direct calculations reveal that this is not the case. In CdSe dots, the β value for CBM is about three times of that for VBM, seemingly consistent with the fact that m_e^* is about one third of the m_h^* . However, this is just a coincident. In CdS dots, m_e^* is only one quarter of m_h^* . If β is inversely proportional to the effective mass, we anticipate for CdS dots that β should be larger for the CBM than for the VBM, like the CdSe dots in Table IV. However, our direct calculation results in Table IV show the opposite, and β_{CBM} is many folds smaller than β_{VBM} .

To study individual contributions from the CBM and from the VBM to the opening of band gap, we use the ratio between the confinement energy of the CBM and that of the VBM, defined as

$$Q(D) = \frac{\varepsilon_{\text{CBM}}^{\text{QD}} - \varepsilon_{\text{CBM}}^{\text{Bulk}}}{\varepsilon_{\text{VBM}}^{\text{Bulk}} - \varepsilon_{\text{VBM}}^{\text{QD}}} . \quad (4)$$

In CdS dots, we find that Q *increases* almost linearly with the increasing size, from being 2.2 for the $r=2.0a_0$ dot to 5.5 for the $r=4.5a_0$ dot. However, in the case of CdSe dots, this ratio fluctuates—within $\pm 10\%$ —around an average value of 1.7. We thus see that in both QDs the major contribution to the opening of the band gap arises from the upward shift of the CBM rather than the downward shift of the VBM. This conclusion is, in a qualitative sense, consistent with the simple effective mass theory. However, and as discussed above, an attempt to quantitatively interpret our pseudopotential results using the effective mass theory leads to large errors and is questionable. The significant difference, exhibited by CdSe and CdS dots, in the size dependence of the Q ratio could be understood by use of Eq.(3) and the parameters in Table IV, which leads to $Q(D) = 0.1368D$ (a linear relation) for CdS dots and $Q(D) = 2.4631/D^{0.1}$ (a very weak size dependence) for CdSe dots. In recent TB calculations,[14] it was shown that the CBM contribution to the band gap opening is many folds larger than that of the VBM for II-VI QDs in the size range of 7-70Å in diameter, in accord with our results. Both theoretical results differ from the conclusion deduced from the spectroscopy experiment [29] where the size confinement was found to open the band gap in CdS QDs with nearly equal contributions from the CBM and VBM. This discrepancy could be due to the poor surface passivation in experiment [29], which may lead to surface electron states showing different size dependence as compared to bulklike band-edge states.

(4) In our computational scheme, since the experimental work functions of bulk CdSe and CdS were used to construct our SEPM pseudopotentials, the absolute energy levels in

the calculations for quantum dots are meaningful, describing the electron orbital energy with respect to the vacuum level. This offers a certain advantage, and makes it possible to conduct a direct comparison of the absolute single-particle energy levels in QDs of two materials. Our SEPM band structure calculations for the *bulks* show that the CBM is higher in CdS than in CdSe by 0.28 eV, while the VBM in CdS is lower by around 0.52 eV. These values are, in fact, the natural band offset obtained from the SEPM pseudopotentials. It would be of interest to examine how these natural band offsets change in dots. In Fig.5, we present the size evolution of the band offsets in dots of two materials, i.e., the energy difference between the band edge states in two types of QDs. In Fig.5 the upper and lower bounds of the figure represent the bulk limits. We exclude the VBM of the smallest $r=2.0a_0$ QD from the consideration due to the energy crossover in CdSe QD. We can clearly see that $\Delta(\text{CBM})$ is approaching the bulk limit as size increases, similarly with the $\Delta(\text{VBM})$. Strictly speaking, no conclusion should be made about the variation of either quantity outside the size window considered here. The key conclusion in Fig.5 is that both the conduction and valence band offsets decrease when size decreases. The curve of the VBM band offset in Fig.5 shows more complexity than the CBM curve, reflecting the multiple level crossings as well as quantum size effects on the VBs in two QDs.

Interband, intraband transitions and optical properties: To characterize optical properties of the CdSe and CdS QDs, we calculate the transition matrix elements between the single particle levels as

$$T_i = |\langle \psi_e | \hat{r}_i | \psi_h \rangle|^2 \quad (5)$$

where $i = x, y, z$ is the polarization direction. In Fig.6 we present the size dependence of the total transition probability ($T_1+T_2+T_3$) calculated for the transitions between the CBM and the VBM. The main observations are: (i) In all sizes shown, the VBM-to-CBM transition is dipole allowed in both QDs. This is in contrast with a previously reported study on CdS QDs which showed that the VBM has a p -like envelope symmetry and is optically forbidden to the CBM [17]. (ii) Apart from the smallest CdSe dot, the transition probability shows a monotonic increase as size increases. The slight increase in the smallest CdSe QD is due to the level crossover between the VBM and VBM-1. If we correct for that level crossover in the smallest CdSe QD by incorporating the CBM to the VBM-1 transition, we obtain an almost linear relation similar to that of CdS. (iii) Interestingly, the total dipole transition strength is larger in CdS QDs than in CdSe dots of the same size.

To further explore the optical properties of these systems, we also present in Fig.7 the size evolution of the optical transitions between the CBM and the highest four VB states below the VBM. These valence states are of particular relevance because they are close to the VBM. Inspecting first the transition from the CBM to the next highest VBM-1 state shown in Fig.7(a), we can see clearly that this transition is strongly allowed for the smallest four sizes in both CdSe and CdS. However, for the two largest sizes, we notice a sudden and sharp drop of the transition probability in the CdS QDs, and a smoother drop in the CdSe QDs that eventually transforms this transition into an optically forbidden one. The reason for this drop is due to a change in the nature of the VBM-1 into a p -like state. In CdSe QDs, and as confirmed by the wavefunction analysis, we notice that as size increases, the VBM-1 (s -like) of the $r=3.5a_0$ dot evolves into the VBM-3 in the $r=4.0a_0$ and $r=4.5a_0$ dots. Indeed, one can see by combining Fig.7(a) and Fig.7(c) that as the transition probability decreases between VBM-1 and CBM, the probability between VBM-3 and CBM arises. In other words, the probability between VBM-1 and CBM in $r=3.5a_0$ is transferred to the transition between VBM-3 and CBM in $r=4.5a_0$. A similar situation occurs for the CdS QDs but differs in the details of the level crossings: the VBM-1 (s -like) of the $r=3.5a_0$ dot becomes the VBM-2 in the $r=4.0a_0$ QD, and then subjects to another level crossing and is changed into the VBM-3 in the $r=4.5a_0$ dot. As this happens, the VBM-2 in the $r=4.0a_0$ dot, and the VBM-3 in the $r=4.5a_0$ dot, should be allowed. This is consistent with the fact that the transition probability is indeed large for the $r=4.0a_0$ dot in Fig.7(b), and for the $r=4.5a_0$ dot in Fig.7(c). One may further ask why the change in the optical transition probability between the VBM-1 and the CBM is smooth in CdSe dots but abrupt in CdS dots, as shown in Fig.7(a). A careful examination of individual wave functions for both material QDs reveals another significant difference that could resolve the issue. In CdS QDs, the VBM-1 state of the two largest sizes has a more pronounced p -component when compared to its counterpart in CdSe dots. As shown in the last row of Fig.4, the VBM-1 in the $r=4.5a_0$ dot (evolved from the VBM-3 of the $r=3.5a_0$) still has some contribution at the center of the QD. This arises from a significant interstate mixing with nearby s -like VB states. In the case of the CdS dots, for the VBM-1 of the two largest QDs, the wavefunctions show zero contribution in the central region of the QD, an indication of stronger p -nature, thus explaining the weaker optical transition probability.

We next investigate the intraband transitions. The intraband transitions inside the con-

duction band provide access to transitions with wave lengths in the energy regime from middle to far infrared. The cascade lasers utilize engineered structures of quantum wells that can generate wavelengths in this regime through sub-band electronic transitions in their CB bands. The demand for new materials and structures that can provide such type of infrared emission is high. The intraband transitions in CdSe and/or CdS dots offer an interesting alternative. Indeed, for the size range we study here, the transition between the CBM and the CBM+1 covers the wave length from 1.8 to 4 μm for the case of CdSe QDs. In Fig.8, we show the size evolution of the probability of intraband transitions from the CBM to the low lying CB states. The main results are: (i) These transitions are allowed, with transition amplitude being about one quarter of the band edge transition or other inter-band transitions. Meanwhile, since the CBM+1, CBM+2 and CBM+3 are close in energy, the total intensity of intraband transitions (i.e., with density of states accounted for) is not small, offering a promising application of utilizing these CB transitions for infrared devices. (ii) Unlike Fig.6 where the intensity of the interband VBM-to-CBM transition increases with the size, the size evolution of the CBs-CBs intraband transitions does not show a monotonic behavior. Interestingly, the intraband transitions in Fig.8 peak at a size between 22 and 30 \AA for CdSe and CdS QDs. This tells us that there may exist an optimal nanocrystal size that could generate maximum intraband transition intensity for infrared applications. (iii) While for *interband* transitions the dipole strengths are slightly higher in CdS dots than in CdSe dots, the opposite is true for *intraband* transitions. We see in Fig.8 that CdS dots generally have a weaker intraband transitions than CdSe dots. The more localized conduction wavefunctions in CdS dots may be responsible for this predicted result.

Electron-hole interactions and exciton gap: Figure 9 presents the calculated magnitude of the Coulomb binding energy between the electron at CBM and hole at VBM in different sizes of QDs. The two curves in Fig.9 show similar behavior. The Coulomb interaction is shown to sharply decrease when going from the smallest to the largest size, and is best fit by $E_{\text{Coul}} = \text{Constant}/D^\gamma$ where γ is found to be 1.54 (1.45) for CdSe (CdS) QDs. Notably, even for the largest dot, the e-h Coulomb attraction energy ($\sim 200\text{meV}$) is far stronger than in bulk where the Coulomb energy is about 20meV. As a result, the electron-hole pairs in CdSe or CdS dots are very stable against thermal fluctuation. Comparing CdS with CdSe QDs in Fig.9, the Coulomb binding is larger by about 65 meV in the smallest CdS dot than in the smallest CdSe dot. This difference shrinks as size increases, becoming ~ 20 meV for

the largest QD.

In order to examine whether or not the Coulomb interaction may change the level ordering between the ground-state exciton and next higher-energy exciton, we also pay special attention to the Coulomb binding between VBM-1 and CBM. We find (not shown here) that in the case of CdSe QDs, the Coulomb interaction of the CBM with the VBM is always larger than that with the VBM-1, the difference being a few meVs for the smallest four QD sizes and then increasing to 15.5 meV for the largest size. Consequently, the e-h pair between VBM and CBM in CdSe dots remains to be the ground-state exciton even when Coulomb interaction is considered. In the case of the CdS QDs, the situation is slightly different. We find that for the two largest sizes, the Coulomb binding between VBM and CBM is larger than that between VBM-1 and CBM by ~ 22 meV, thus preserving the order of two lowest excitons. However, for the four smallest CdS dots, the Coulomb interaction between VBM-1 and CBM becomes stronger than that of the CBM-VBM exciton, but by only ~ 2 meV. Since the single-energy level between VBM and VBM-1 in the inset of Fig.3 is ~ 40 meV, much larger than the magnitude of 2meV difference due to the Coulomb interaction, we conclude that inclusion of the e-h Coulomb energy, once again, does not change the order of *s/p*-excitons.

The exchange interaction, shown in the inset of Fig.9 for the QDs of two materials, is essentially more than an order of magnitude smaller than the Coulomb interaction. Our results indicate that the exchange energy decreases with size in a faster rate than the Coulomb term, and approaches the bulk limit (around 0.1 meV) for large QDs. In the case of the smallest CdS QD, the obtained CBM-VBM exchange interaction is 12 meV. For the smallest CdSe QD, this value is around 11 meV. However, if we correct for the crossover at the top of the VB in the smallest size (by considering the next excitonic configuration formed by the VBM-1 state and the CBM), the exchange interaction jumps to around 17 meV. This clearly indicates the significant effect of size confinement on the exchange interaction.

In the strong confinement regime, the exchange interaction (and also the correlation effect) are very small. Thus we can describe the energy of the ground state exciton by the expression: $E_{ex} = (\epsilon_{CBM} - \epsilon_{VBM}) - E_{Coul}$. The size evolution of the excitonic gap is depicted in the top panel of Fig.10 for CdSe dots, and in the bottom panel for CdS dots. Our direct calculated values (gray solid circles) are shown in comparison with available experimental and theoretical data. The figure reveals an overall excellent agreement between our theory

and experiments. The solid lines in Fig.10 represent the best fit for the variation of the excitonic gap with the diameter of the QD by using

$$E_{ex}(\text{Dot}) = E_{ex}(\text{Bulk}) + \frac{\tau}{D^\mu} . \quad (6)$$

The fitting parameters we obtained are: τ is 69.2 for CdSe and 63.0 for CdS dots, and μ is 1.42 for CdSe and 1.46 for CdS dots. As a comparison, we present in the bottom panel of Fig.11 the confinement energy—namely, $E_{ex}(\text{Dot}) - E_{ex}(\text{Bulk})$ —of the ground-state exciton in CdSe and CdS dots, using the scaling law of Eq.(6). As can be clearly seen, for the same QD size, the confinement energy of the ground-state exciton is higher in the CdSe dots for the size range considered here. The difference is about 100 meV. The larger confinement energy in CdSe dots can be qualitatively understood as follows. In bulk CdSe, the smaller band gap allows strong coupling between valence states and conduction states. As the result of this strong coupling, the band dispersion shows larger curvature (thus producing smaller effective masses). When forming quantum dots, the bulk dispersion is folded back to the Γ point, and larger dispersion in bulk CdSe will lead to larger confinement energy. In a previous report, Li and Wang used the charge patching method to study the exciton energies as a function of the size.[31] Their exciton confinement energies of CdSe and CdS QDs are shown in the inset of the lower panel of Fig.11. They also found that the confinement energy in CdSe QDs is greater than in CdS QDs, in agreement with our results though the details of the energies slightly differ. Some people prefer an alternative way to examine the exciton confinement energy, namely, by rescaling the size of the dot according to the exciton Bohr radius (R_{ex}) of the bulk. In other words, one plots the confinement energy versus the normalized size D/D_{ex} ($D_{ex} = 2.0R_{ex}$). The result is shown in the top panel of Fig.11. Since $R_{ex}=55\text{\AA}$ of CdSe is much larger than $R_{ex}=25\text{\AA}$ of CdS, the scaled size D/D_{ex} falls in between 0.15 and 0.35 for CdSe dots, far less than that for CdS dots (where D/D_{ex} is between 0.3 and 0.7). The confinement energy in this normalized size scheme turns out to be large in CdS QDs. Nevertheless, we need to keep in mind that in the top panel of Fig.11 we are not comparing the CdSe and CdS dots of the same size.

IV. CONCLUSIONS

We have performed a comparative theoretical study on various properties in CdSe and CdS dots. For this purpose, we first derived from first-principles density functional calculations the screened atomic pseudopotentials for CdS as well as for CdSe, so that the comparison can be made on equal footing. The screened atomic pseudopotentials and passivations were then used to determine electronic and optical properties in each type of quantum dots. The properties we investigated include single-electron energy levels, characterization of individual wavefunctions, interband transitions, intraband transitions, electron-hole Coulomb and exchange interactions, and exciton gap. Our main findings are summarized in the following. (i) The conduction state spectrum is similar in CdSe and CdS dots. In both dots, we found two intraband gaps inside the conduction band. The CBM is separated from the next three CB states (CBM+1, CBM+2, CBM+3) by an intraband gap $\Delta E_{\text{intra,CB}}^{(1)}$. The CBM+3 is separated from the higher conduction states by another intraband gap $\Delta E_{\text{intra,CB}}^{(2)}$. $\Delta E_{\text{intra,CB}}^{(1)}$ shows a significant dependence on size, and $\Delta E_{\text{intra,CB}}^{(2)}$ does not. (ii) The valence state spectra in CdSe dots and in CdS dots exhibit differences, manifested by the fact that there is one intraband gap in the former but apparently two intraband gaps in the latter. The magnitude of the intraband gaps and the size dependence are also different, as shown in Fig.3. The difference in the valence states between CdSe and CdS dots is attributed to the large spin-orbit coupling in CdSe, which to some extent decouples the spin-split band from the top valence bands and thus reduces interstate coupling. (iii) The VBM state in CdS dots is found to have *s*-like envelope symmetry. This state is transition allowed to the CBM. (iv) According to our direct calculations, the single particle orbital energy depends on size by, $\varepsilon_{\text{CBM}}^{\text{dot}} = \varepsilon_{\text{CBM}}^{\text{bulk}} + 83.5/D^{1.5}$ and $\varepsilon_{\text{VBM}}^{\text{dot}} = \varepsilon_{\text{VBM}}^{\text{bulk}} + 33.9/D^{1.4}$ for CdSe dots, and $\varepsilon_{\text{CBM}}^{\text{dot}} = \varepsilon_{\text{CBM}}^{\text{bulk}} + 36.9/D^{1.2}$ and $\varepsilon_{\text{VBM}}^{\text{dot}} = \varepsilon_{\text{VBM}}^{\text{bulk}} + 269.7/D^{2.2}$ for CdS dots. These analytic expressions should be of some useful values to experimental measurements and other theoretical calculations. (v) The $Q(D)$ quantity, which describes the confinement-induced shift of the CBM with respect to that of the VBM, shows little size dependence and is around 1.7 for CdSe dots. But for CdS dots, $Q(D)$ is found to depend linearly on *D*, increasing from 2.2 to 4.8 for the size range considered. (vi) The natural band offset between CdSe and CdS dots of the same size decreases with the size, as described in Fig.5. The band offset for VBM is more complex than that for CBM due to level crossing. (vii) The dipole matrix strength

of the VBM→CBM interband transition increases with size. But the dipole strength of intraband transitions within the conduction states shows a non-monotonous dependence on size and peaks around $D=25\text{-}30\text{\AA}$. (viii) Our calculations reveal that the *interband* dipole strength is considerably larger in CdS dots than in CdSe dots. But the opposite is true for *intraband* dipole strength, which is larger in CdSe dots. Nevertheless, the intraband dipole strength in both dots is large enough, promising for infrared applications. (ix) The e-h Coulomb binding in both dots is strong, being about 200 meV in $D=37\text{\AA}$ dot which far exceeds the value of ~ 20 meV in bulk. For the same size, the e-h Coulomb binding is slightly stronger in CdS dots than in CdSe dots (see Fig.9). (x) Our calculated exciton energies agree well with experimental measurements and/or other theoretical calculations. Our calculated confinement induced shift of exciton energy is $E_{ex}(\text{Dot}) - E_{ex}(\text{Bulk}) = 69.2/D^{1.42}$ for CdSe dots and $E_{ex}(\text{Dot}) - E_{ex}(\text{Bulk}) = 63.0/D^{1.46}$ for CdS dots. When the size is the same, the exciton confinement energy in CdSe dot is found to be larger than that in CdS dot.

We thank Professor Xiaogang Peng for helpful discussions. This work was supported by the Oklahoma-Arkansas MRSEC.

-
- [1] Al. L. Efros and A. L. Efros, Sov. Phys. Semicond. **16**, 772 (1982). For a review, see Al. L. Efros and M. Rosen, Annu. Rev. Mater. Sci. **30**, 475 (2000)
 - [2] L. E. Brus, J. Chem. Phys. **79**, 5566 (1983).
 - [3] D. Schooss, A. Mews, A. Eychmuller and H. Weller, Phys. Rev. B **49**, 17072 (1994).
 - [4] V. A. Fonoberov, E. P. Pokatilov, and A. A. Balandin, Phys. Rev. B **66**, 085310 (2002).
 - [5] H. Fu, L.-W. Wang and A. Zunger, Phys. Rev. B **57**, 9971 (1998).
 - [6] J. Li and J. B. Xia, Phys. Rev. B **61**, 880 (2000).
 - [7] L.-W. Wang and A. Zunger, Phys. Rev. B **51**, 17398 (1995).
 - [8] J. Hu, L.-S. Li, W. Yang, L. Manna, L.-W. Wang and A. P. Alivisatos, Science **292**, 2060 (2001).
 - [9] K. Leung, S. Pockrant and K. B. Whaley, Phys. Rev. B **57**, 12291 (1998).
 - [10] S. Pokrant and K. B. Whaley, Eur. Phys. J. D **6**, 255 (1999).
 - [11] Jesús Pérez-Conde and A. K. Bhattacharjee, Phys. Rev. B **63**, 245318 (2001).
 - [12] U. E. H. Laheld and G. T. Einevoll, Phys. Rev. B **55**, 5184 (1997).

- [13] J. Li and J. B. Xia, Phys. Rev. B **62**, 12613 (2000).
- [14] Sameer Sapra and D. D. Sarma, Phys. Rev. B **69**, 125304 (2004).
- [15] C. B. Murray, C. R. Kagan and M. G. Bawendi, Annu. Rev. Mater. Sci. **30**, 545 (2000).
- [16] S. A. Empedocles, R. Neuhauser, K. Shimizu and M. G. Bawendi, Adv. Mater. **11**, 1243 (1999).
- [17] Z. Yu, J. Li, D. B. Oconnor, L.-W. Wang and P F. Barbara , J. Phys. Chem. B **107**, 5670 (2003).
- [18] V. I. Klimov, J. Phys. Chem. B **104**,6112 (2000).
- [19] A. P. Alivisatos, Science (Washington, D. C.) **271**, 933-7 (1996).
- [20] C. B. Murray, D. J. Norris, and M.G. Bawendi, J. Am. Chem. Soc. **115**, 8706 (1993).
- [21] Z. A. Peng and X. Peng, J. Am. Chem. Soc. **123**, 183 (2001).
- [22] *Semiconductors, Physics of Group II-VI and I-VII compounds, Semimagnetic, Semiconductores*, edited by K.-H. Hellwege and O. Madelung, Landolt-Bornstein, New Series, Group III, Vol. **17-B**, Springer- Verlag, Berlin, (1982).
- [23] D.J. Norris and M.G. Bawendi, Phys. Rev. B **53**, 16338 (1996).
- [24] D. Bertram, O.I. Micic, and A.J. Nozik, Phys. Rev. B **57**, R4265 (1998).
- [25] R.J. Ellingson, J.L. Blackburn, J. Nedeljkovic, G. Rumbles, M. Jones, H. Fu, and A.J. Nozik, Phys. Rev. B **67**, 075308 (2003).
- [26] D. O. Demchenko and L.-W. Wang, Phys. Rev. B **73**, 155326 (2006).
- [27] T. van Buuren, L.N. Dinh, L.L. Chase, W.J. Siekhaus, and L.J. Terminello, Phys. Rev. Lett. **80**, 3803 (1998).
- [28] F.A. Reboredo, A. Franceschetti, and A. Zunger, Phys. Rev. B **61**, 13073 (2000); G. Allan, C. Delerue, and M. Lannoo, Phys. Rev. Lett. **78**, 3161 (1997).
- [29] J. Lüning, J. Rockenberger, S. Eisebitt, J.-E. Rubensson, A. Karl, A. Kornowski, H. Weller and W. Eberhardt, Sol. State Comm. **112**, 5 (1999).
- [30] P. Guyot-Sionnest, M. Shim, C. Matranga and M. Hines, Phys. Rev. B **60**, R2181 (1999).
- [31] J. Li and L.-W. Wang, Phys. Rev. B **72**, 125325 (2005).
- [32] A. Mizel and M. L. Cohen, Phys. Rev. B **56**, 6737 (1997).
- [33] W. Kohn and L.J. Sham, Phys. Rev. **140**, A1133 (1965).
- [34] M.S. Hybertsen and S.G. Louie, Phys. Rev. B **34**, 5390 (1986).
- [35] F. Buda, J. Kohanoff, and M. Parrinello, Phys. Rev. Lett. **69**, 1272 (1992).

- [36] X. Zhao, C.M. Wei, L. Yang, and M.Y. Chou, *Phys. Rev. Lett.* **92**, 236805 (2004).
- [37] W. Su, X. Huang, J. Li, and H. Fu, *J. Am. Chem. Soc.* **124**, 12944 (2002).
- [38] J. Li and L.-W. Wang, *Phys. Rev. B* **72**, 125325 (2005).
- [39] N.A. Hill and K.B. Whaley, *Phys. Rev. Lett.* **75**, 1130 (1995).
- [40] G.W. Bryant and W. Jaskolski, *Phys. Rev. B* **67**, 205320 (2003).
- [41] G. Allan and C. Delerue, *Phys. Rev. B* **70**, 245321 (2004).
- [42] L.-W. Wang, and A. Zunger, *J. Chem. Phys.* **100**, 2349 (1994).
- [43] A. Franceschetti and A. Zunger, *Phys. Rev. Lett.* **78**, 915 (1997).
- [44] L.W. Wang and A. Zunger, *Phys. Rev. B* **59**, 15806 (1999).
- [45] P.C. Sercel and K.J. Vahala, *Phys. Rev. B* **42**, 3690 (1990).
- [46] Al. L. Efros and M. Rosen, *Annu. Rev. Mater. Sci.* **30**, 475 (2000)
- [47] H. Fu and A. Zunger, *Phys. Rev. B* **56**, 1496 (1997).
- [48] J. Li and L.-W. Wang, *Nano Letters* **3**, 1357 (2003).
- [49] L.-W. Wang and A. Zunger, *J. Phys. Chem. B* **102**, 6449 (1998).
- [50] A. Franceschetti, H. Fu L.-W. Wang and A. Zunger, *Phys. Rev. B* **60**, 1819 (1999).
- [51] L.-W. Wang and A. Zunger, *Phys. Rev. Lett.* **73**, 1039 (1994).
- [52] M. C. Payne, M. P. Teter, D. C. Allan, T. A. Arias, and J. D. Joannopoulos, *Rev. Mod. Phys.* **64**, 1045 (1992).
- [53] A. Puzder, A. J. Williamson, F. Gygi, and G. Galli, *Phys. Rev. Lett.* **92**, 217401 (2004).
- [54] L.-W. Wang and A. Zunger, *Phys. Rev. B* **53**, 9579 (1996).
- [55] S. A. Empedocles, D. J. Norris, and M. G. Bawendi, *Phys. Rev. Lett.* **77**, 3873 (1996).
- [56] C. R. Kagan, C. B. Murray, and M. G. Bawendi, *Phys. Rev. B* **54**, 8633 (1996).
- [57] C. R. Kagan, C. B. Murray, M. Nirmal, and M. G. Bawendi, *Phys. Rev. Lett.* **76**, 1517 (1996).
- [58] T. Vossmeier, L. Katsikas, M. Giersig, I. G. Popovic, K. Diesner, A. Chemseddine, A. Eychmueller, and H. Weller, *Phys. Chem.* **98**, 7665 (1994).
- [59] Yu.P. Rakovich, M.V. Artemyev, A.G. Rolo, M.I. Vasilevskiy, M.J.M. Gomes, *Physica Status Solidi (b)* **224**, 319 (2001).

TABLE I: Parameters of passivation potentials for CdS and CdSe quantum dots.

CdS						
1 Dangling Bond			2 Dangling Bonds			
	V_0 (Hartree)	d(Bohr)	R(Bond length)	V_0 (Hartree)	d(Bohr)	R(Bond length)
Cd	-4.00	1.00	1/4	-9.00	0.70	1/3
S	-3.00	0.80	1/4	-4.00	0.70	1/4
CdSe						
1 Dangling Bond			2 Dangling Bonds			
	V_0 (Hartree)	d(Bohr)	R(Bond length)	V_0 (Hartree)	d(Bohr)	R(Bond length)
Cd	-8.00	0.70	1/4	-7.00	0.70	1/3
Se	-5.00	0.70	1/4	-4.00	0.70	1/4

TABLE II: The fitting α and β quantities for describing the single-particle confinement energies.

Dots	β_{CBM}	α_{CBM}	β_{VBM}	α_{VBM}
CdSe	83.5	1.5	33.9	1.4
CdS	36.9	1.2	269.7	2.2

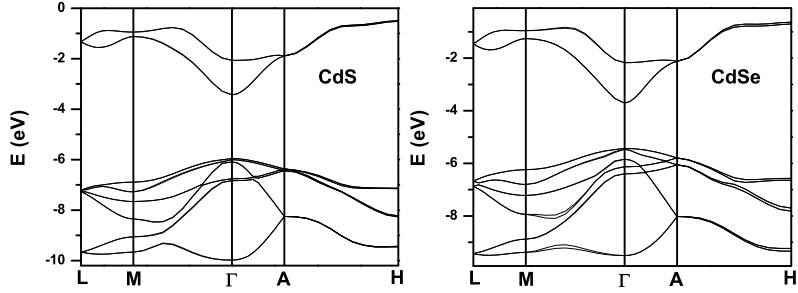


FIG. 1: Theoretical band structure, obtained from the SEPM pseudopotentials, for bulk CdS (left) and CdSe (right) in the wurtzite symmetry. Spin-orbit interaction is included in the calculations.

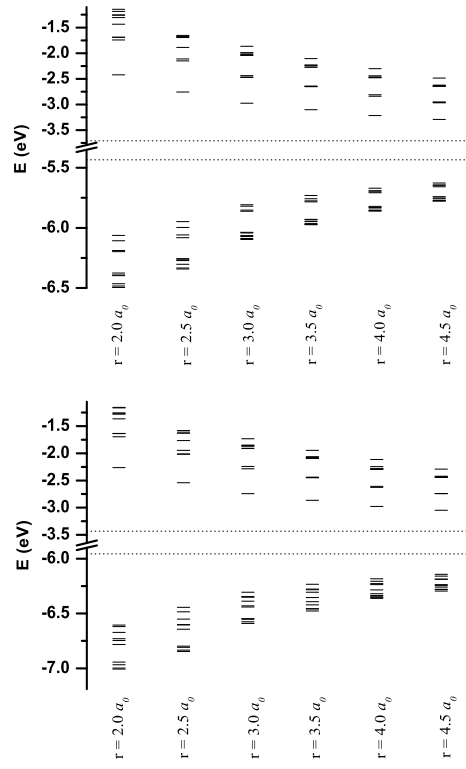


FIG. 2: Calculated single-particle orbital energies for the six considered radius sizes: top panel is for CdSe dots and bottom panel for CdS dots.

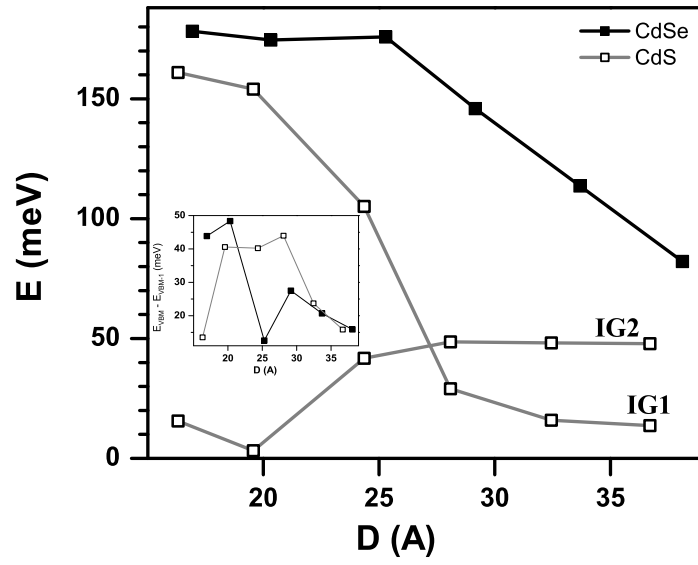


FIG. 3: The size evolution of the VB intraband gaps in both QDs. The filled squares are the CdSe intraband gap separating the highest four VB states from the rest. The two CdS intraband gaps (open squares) are IG1, which separates the highest six VB states from the rest states below, and IG2 which separates the highest four VB states from the rest valence states below. The inset shows the size evolution of the energy separation between the VBM and the VBM-1.

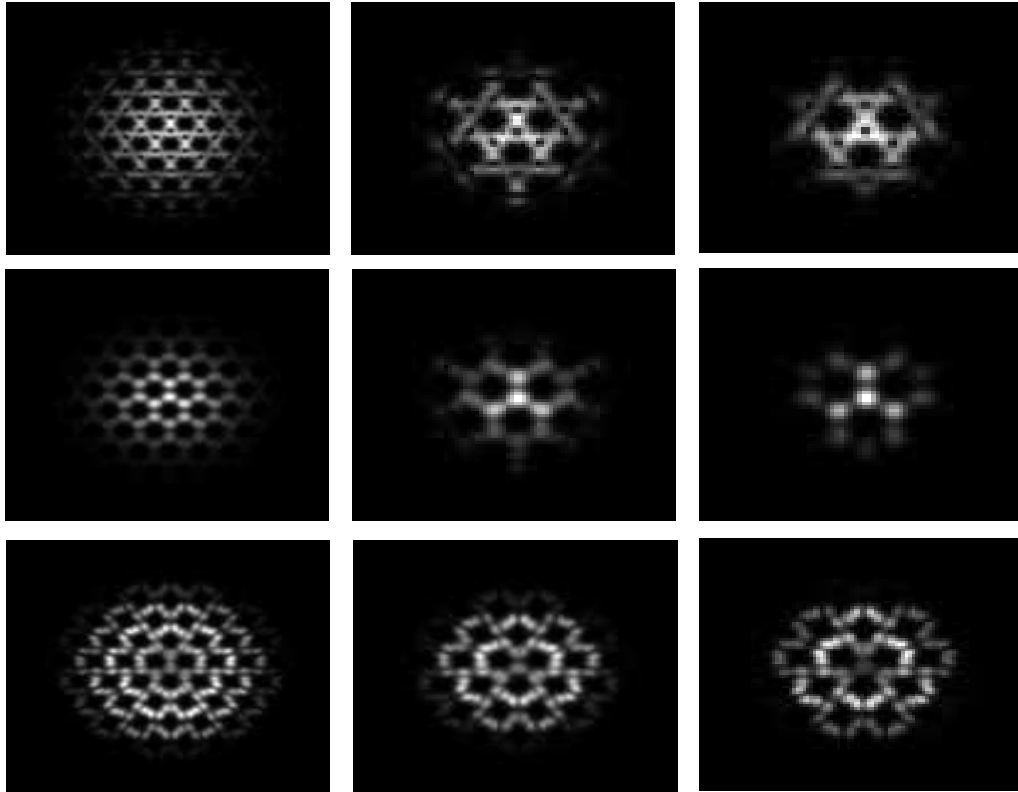


FIG. 4: Wavefunctions squared on the central cross sections in CdSe QDs. Top panel (from left to right): VBM ($r=4.5a_0$), VBM ($r=2.5a_0$), VBM-1 ($r=2.0a_0$); Second panel: VBM-3 ($r=4.5a_0$), VBM-1 ($r=2.5a_0$), VBM ($r=2.0a_0$); Third panel: VBM-1 ($r=4.5a_0$), VBM-3 ($r=3.5a_0$), VBM-2 ($r=3.0a_0$).

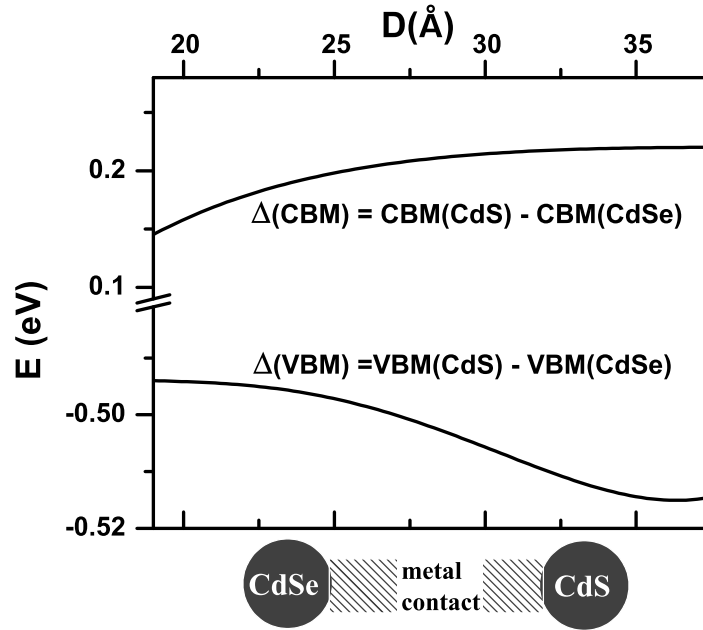


FIG. 5: The size evolution of the natural band offsets in CdS and CdSe QDs. These curves were generated by first fitting the size evolution of the individual band edge state in both CdS and CdSe QDs to a polynomial, and then these polynomials were subtracted from each other to yield the curves in this figure. The upper and lower bounds of the figure are the bulk limits.

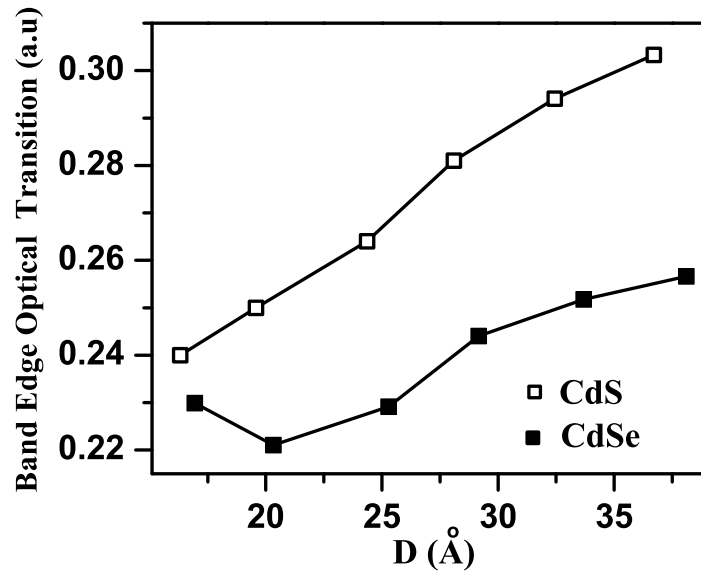


FIG. 6: Calculated optical transition probability (in atomic units) between the VBM and the CBM in different sizes of dots.

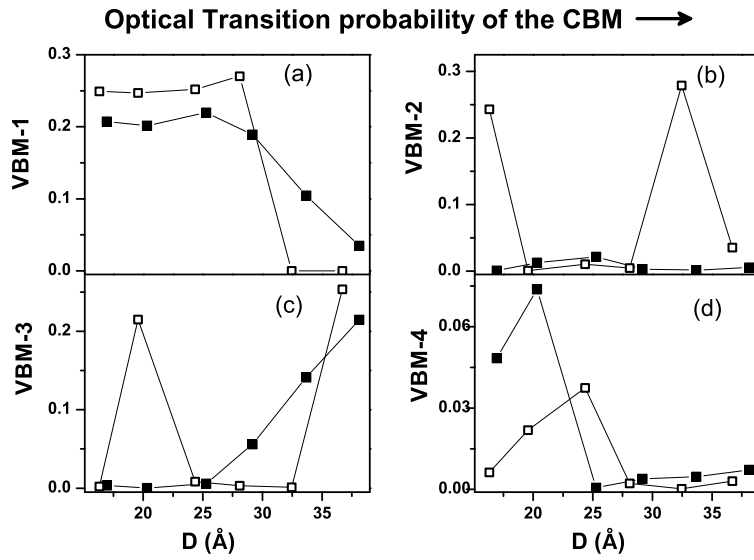


FIG. 7: Calculated optical transition probabilities from the following valence states to the CBM: a) VBM-1, b) VBM-2, c) VBM-3 and d) VBM-4. Filled squares are for CdSe dots, and empty squares are for CdS dots.

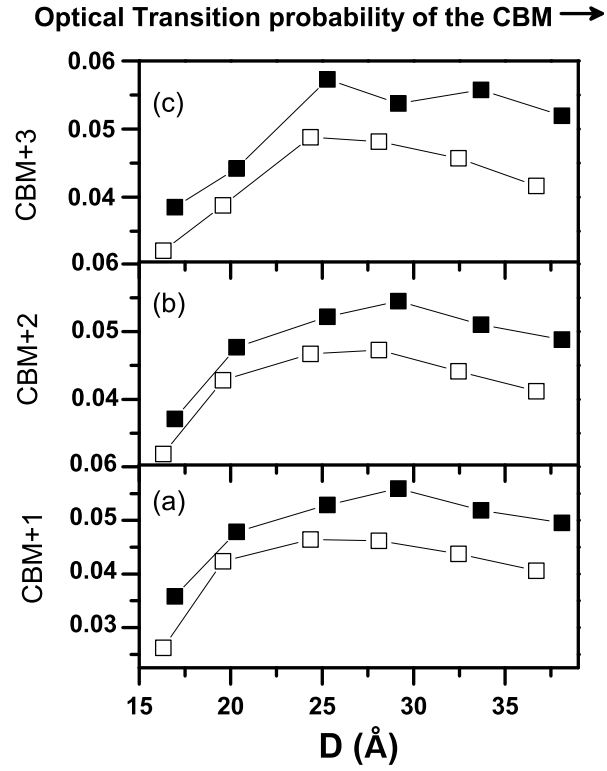


FIG. 8: Calculated optical transition probabilities from the CBM to (a) CBM+1, (b) CBM+2, and (c) CBM+3. Filled (empty) squares are for CdSe (CdS) dots.

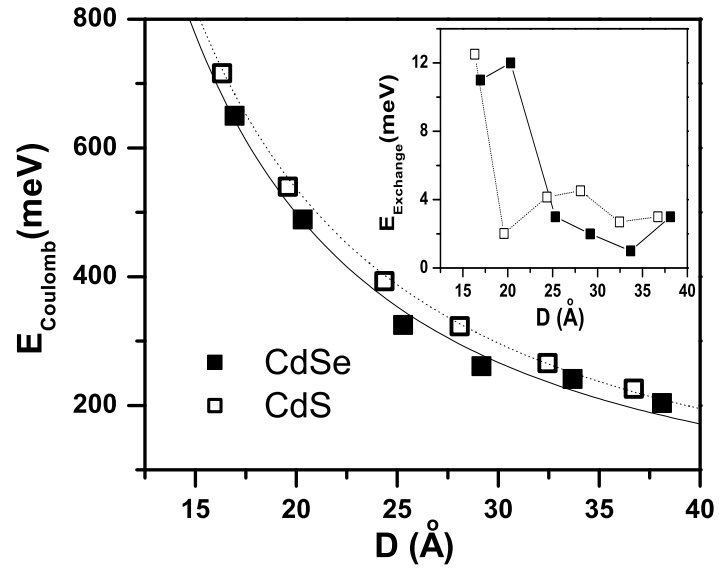


FIG. 9: The size dependency of the Coulomb interaction between VBM and CBM in CdSe and CdS dots. The inset shows the size evolution of the exchange interaction between VBM and CBM.

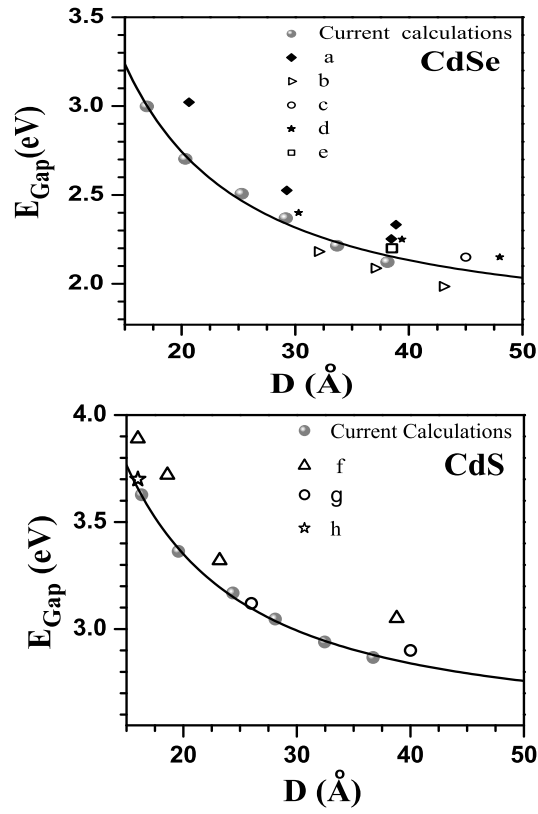


FIG. 10: Size evolution of the excitonic gap in the CdSe (top) and CdS (bottom) QDs. Our calculation results are in solid spheres, compared to experimental and theoretical data extracted from a) references [13, 54], b) [20], c) [55], d) [56], e) [57], f) [58], g) [17], h)[59].

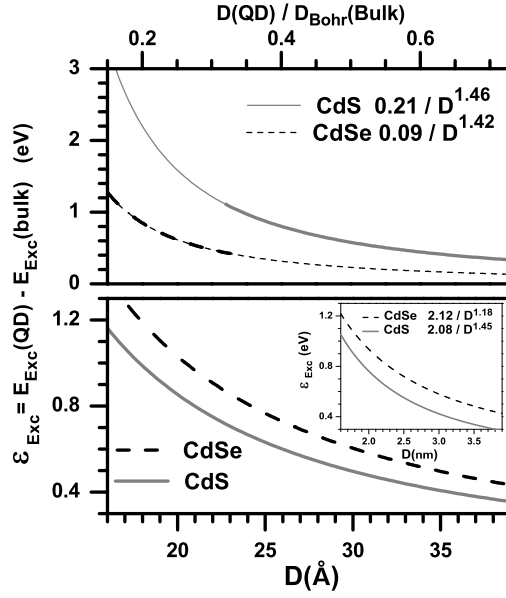


FIG. 11: Lower panel: the size evolution of the ground state excitonic confinement energy relative to the bulk. The inset shows the same quantity obtained from the charge patching calculations [31]. Top panel: the exciton confinement energy as it evolves with the normalized QD size. Note that the thicker lines correspond to the size range of this study.